Available in:
Journal.isrc.ac.ir

Journal of Space Science, Technology& Applications (Persian)

Vol. 6, No. 1, pp.: 117-131
2026

DOI:

10.22034/jssta.2026.537199.1257

Article Info

Received: 2025-08-09
Accepted: 2026-02-15

Keywords

LEO Satellite, System Uncertainty, Attitude Control, AFSMC, Reaction Wheels

How to Cite this article

Z. Tahmasi Jahed, A. H. Davaie Markazi, T. Abdollahi, "Adaptive Fuzzy Sliding Mode Control of Pointing Maneuvers of an Uncertain LEO Communication Satellite", ***Journal of Space Science, Technology& Applications*****, Vol. 6, No. 1, pp. 117-131, 2026.**

Original Article

Adaptive Fuzzy Sliding Mode Control of Pointing Maneuvers of an Uncertain LEO Communication Satellite

Zeinab Tahmasi Jahed [1], Amir Hossein Davaie Markazi [2]*, Taleb Abdollahi [3]

1 Master Student, School of Mechanical Engineering,
Iran University of Science and Technology, Tehran, Tehran, 1684613114, Iran
Zeinabtahmasi1196@gmail.com

2* Professor, School of Mechanical Engineering
Iran University of Science and Technology, Tehran, Tehran, 1684613114, Iran
markazi@iust.ac.ir

3 Assistant Professor, Institute of Mechanics,
Institute of Mechanics, Shiraz, Fars, 71555414, Iran
talebabdollahy@yahoo.com

Abstract

Precise pointing of a Low Earth Orbit (LEO) satellite is vital to maintain the antenna, gimbaled cameras, and solar panels in the correct direction. To address the complexities and uncertainties in the dynamics of a typical low Earth orbit (LEO) satellite equipped with a Ka-band transmitter and to overcome external disturbances, this study introduces an Adaptive Fuzzy Sliding Mode Control (AFSMC) approach, which is shown to be robust against uncertainties with unknown upper bounds. The control input is generated directly by a sliding-mode controller, with an adaptive method used to estimate the upper bound of the uncertainty. In contrast to traditional Sliding Mode Control (SMC), AFSMC integrates an online-estimated fuzzy controller, obviating the need for model-based linearization. The stability of the closed-loop system is rigorously ensured through Lyapunov stability analysis. Comparative simulations against Proportional-Derivative (PD) and SMC controllers highlight the AFSMC's superior pointing accuracy and reduced energy consumption, demonstrating its effectiveness.

1- Introduction

Satellites are integral to modern society, performing essential functions in communication, remote sensing, navigation, and meteorology. However, their operations face significant uncertainties and external disturbances, necessitating robust control systems to ensure optimal performance throughout their operational lifespans.

Research in satellite attitude control dates back to Stuhlinger's pioneering work in 1956. As satellite applications expanded, so did the development of advanced control methods. Early efforts, as discussed by Nobuaki et al. [1], Zwartbol et al. [2], and Mobley et al. [3], primarily focused on implementing classical control algorithms using onboard computers and associated hardware. These methods, however, often required frequent adjustments to mitigate performance degradation caused by external disturbances. Subsequently, advancements in adaptive control techniques emerged. For instance, Geng et al. [4] introduced system identification methods to dynamically tune control parameters based on environmental conditions. In a relatively similar study, Alipour et al. [5] developed an adaptive sliding mode controller to handle small initial deviations. Additionally, incorporating fuzzy inference methods enhanced tolerance to model uncertainties, And in recent years, in a similar study, Liu et al. [6] developed an adaptive fuzzy sliding-mode controller for spacecraft attitude tracking during space-debris removal. However, their study does not specifically address large-angle attitude maneuvers of a rigid LEO spacecraft in a circular orbit.

A review of existing satellite attitude control systems using reaction wheel actuators reveals two primary challenges: (1) non-adaptive control algorithms often lead to performance degradation over time, and (2) frequent parameter adjustments are required to account for environmental variations, which can introduce transient instability or miscalibration.

To address these limitations, this paper presents a novel Adaptive Fuzzy Sliding Mode Control (AFSMC) approach, to control large initial deviations of a rigid spacecraft in a circular LEO orbit, which combines sliding mode, adaptive, and fuzzy logic techniques. The proposed AFSMC controller improves robustness against uncertainties, reduces dependency on precise system modeling, and enhances overall control performance.

While previous studies have applied the AFSMC method to flexible satellites and satellite formations in circular orbits for maneuver control [7, 8], its application to rigid LEO satellites with large initial deviations has not been explored. This paper fills this gap by developing and validating an AFSMC controller specifically for an LEO communication satellite.

The remainder of this paper is structured as follows: Section 2 provides a concise review of the satellite dynamic model and stabilization devices. Section 3 details the proposed AFSMC controller and includes the stability analysis. Section 4 outlines the satellite communication equipment. Section 5 presents simulation results, and Section 6 concludes the paper with final remarks.

2- Dynamic Modelling

2-1- Kinematics

The rotation of the BCS relative to the OCS is the kinematic basis of angular motion. The total satellite angular velocity expressed in the BCS, ω_{IB}^{B}, is presented in Equation 1

$$\boldsymbol{\omega}_{IB}^{B} = \boldsymbol{\omega}_{IR}^{B} + \boldsymbol{\omega}_{RB}^{B} \tag{1}$$

where, ω_{RB}^{B} is the angular velocity of the BCS relative to the OCS expressed in the BCS, and ω_{IR}^{B} is the angular velocity of the OCS relative to the ICS expressed in the BCS. It is fairly standard to show as Equation 2 [9]

$$\omega_{RB}^{B} = \begin{bmatrix} \dot{\phi} - \dot{\psi}\sin\theta \\ \dot{\theta}\cos\phi + \dot{\psi}\cos\theta\sin\phi \\ \dot{\psi}\cos\theta\cos\phi - \dot{\theta}\sin\phi \end{bmatrix} \tag{2}$$

and in Equation 3 we have

$$\begin{bmatrix} \omega_{IR\,x}^{B} \\ \omega_{IR\,y}^{B} \\ \omega_{IR\,z}^{B} \end{bmatrix} = [A]\begin{bmatrix} 0 \\ -\omega_o \\ 0 \end{bmatrix} \tag{3}$$

Where the matrix $[A]$ is defined as Equation 4

$$[A] = \begin{bmatrix} c\psi c\theta & s\psi c\theta & -s\theta \\ -s\psi c\phi + c\psi s\theta s\phi & c\psi c\phi + s\psi s\theta s\phi & c\theta s\phi \\ s\psi s\phi + c\psi s\theta c\phi & -c\psi s\phi + s\psi s\theta c\phi & c\theta c\phi \end{bmatrix} \tag{4}$$

where θ, ϕ, and ψ are the standard Euler angles, and according to the lateral velocity amount of a circular orbit satellite $v_o = \sqrt{\frac{\mu}{R_o}}$, the Satellite orbit angular velocity is presented in Equation 5 as

$$\omega_o = \frac{v_o}{R_o} = \sqrt{\frac{\mu}{R_o^3}} \tag{5}$$

2-1- Dynamics:

The satellite attitude motion can be described by the Equation 6 as [9]

$$\boldsymbol{T} = \dot{\boldsymbol{h}}_{IT}^B = \dot{\boldsymbol{h}}_{BT}^B + \boldsymbol{\omega}_{IB}^B \times \boldsymbol{h}_{BT}^B \tag{6}$$

where $\boldsymbol{h}_{IT}$ is the total angular momentum, and $\boldsymbol{T}$ is the total torque exerted on the satellite. In the continuation, for the sake of notational simplicity, $\boldsymbol{\omega}_{IB}^B$ will be replaced by $\boldsymbol{\omega}$. The satellite angular momentum relative to the BCS is presented in Equation 7 and consists of two major components: the momentum of the rigid body, $\boldsymbol{h}_B^B$, and the momentum of any exchange devices installed on the spacecraft, $\boldsymbol{h}_W^B$, i.e.,

$$\mathrm{h}_{\mathrm{BT}}^{\mathrm{B}} = \mathrm{h}_{\mathrm{B}}^{\mathrm{B}} + \mathrm{h}_{\mathrm{w}}^{\mathrm{B}} \tag{7}$$

Now define: $[T_{cx} \quad T_{cy} \quad T_{cz}] = [-\dot{h}_{wx} \quad -\dot{h}_{wy} \quad -\dot{h}_{wz}]$, then it is fairly standard to show in Equation 8 that

$$\begin{aligned}
&\boldsymbol{T} = \boldsymbol{T}_c + \boldsymbol{T}_{dis} = \\
&[\dot{h}_x + (\omega_y h_z - \omega_z h_y) + (\omega_y h_{wz} - \omega_z h_{wy})]\hat{\imath} \\
&+[\dot{h}_y + (\omega_z h_x - \omega_x h_z) + (\omega_z h_{wx} - \omega_x h_{wz})]\hat{\jmath} \\
&+[\dot{h}_z + (\omega_x h_y - \omega_y h_x) + (\omega_x h_{wy} - \omega_y h_{wx})]\hat{k}
\end{aligned} \tag{8}$$

Here, the parameters h_{wx}, h_{wy} and h_{wz} represent the nominal momentum of reaction wheels, and $\dot{\mathrm{h}}_{\mathrm{x}} = \mathrm{I}_{\mathrm{xx}}\dot{\omega}_{\mathrm{x}}$, $\dot{\mathrm{h}}_{\mathrm{y}} = \mathrm{I}_{\mathrm{yy}}\dot{\omega}_{\mathrm{y}}$ and $\dot{\mathrm{h}}_{\mathrm{z}} = \mathrm{I}_{\mathrm{zz}}\dot{\omega}_{\mathrm{z}}$ which are in the direction of the BCS axes. By inserting Equation 1 into Equation 8 it can be deduced in Equation 9 that

$$\begin{aligned}
\ddot{\phi} &= \frac{1}{I_{xx}}[T_{cx} + T_{disx} - R_1(\phi, \theta, \psi, \dot{\phi}, \dot{\theta}, \dot{\psi})] \\
\ddot{\theta} &= \frac{1}{I_{yy}\cos\phi}[T_{cy} + T_{disy} - R_2(\phi, \theta, \psi, \dot{\phi}, \dot{\theta}, \dot{\psi})] \\
\ddot{\psi} &= \frac{1}{I_{zz}\cos\phi\cos\theta}[T_{cz} + T_{disz} - R_3(\phi, \theta, \psi, \dot{\phi}, \dot{\theta}, \dot{\psi})]
\end{aligned} \tag{9}$$

By considering small deviations, e.g., less than 3 degrees, after simplifying Equation 4 and then Equation 1, the simplified form of Equation 9 is obtained as Equation 10, which can be used only for small-angle deviations in attitude analysis

$$\begin{aligned}
\ddot{\phi} &= \dot{\psi}\omega_o + \frac{(I_{zz} - I_{yy})}{I_{xx}}\dot{\psi}\omega_o + \frac{4(I_{zz} - I_{yy})}{I_{xx}}\phi\omega_o^2 + \frac{T_{cx} + T_{disx}}{I_{xx}} \\
\ddot{\theta} &= -\frac{3(I_{xx} - I_{zz})}{I_{yy}}\omega_o^2\theta + \frac{T_{cy} + T_{disy}}{I_{yy}} \\
\ddot{\psi} &= -\dot{\phi}\omega_o - \frac{(I_{yy} - I_{xx})}{I_{zz}}(\psi\omega_o^2 - \dot{\phi}\omega_o) + \frac{T_{cz} + T_{disz}}{I_{zz}}
\end{aligned} \tag{10}$$

To utilize Equation 9 in the controller design, it must first be converted into the standard form of a MIMO system equation. For the intended satellite with three second-order derivative outputs, the standard equation is as Equation 11 [9, 10]

$$\boldsymbol{y}^{(2)} = \boldsymbol{F}(\boldsymbol{x}) + \boldsymbol{G}\boldsymbol{u} + \boldsymbol{d} \tag{11}$$

The elements of Equation 11 are expressed in Equation 12 as

$$\begin{aligned}
&\boldsymbol{y} = [y_1 \quad y_2 \quad y_3]^T = [\phi \quad \theta \quad \psi]^T \epsilon\, \mathbb{R}^3 \\
&\boldsymbol{y}^{(k)} = \boldsymbol{y}^{(2)} = [y_1^{k_1} \quad y_2^{k_2} \quad y_3^{k_3}]^T = [\phi^{(2)} \quad \theta^{(2)} \quad \psi^{(2)}]^T \\
&\mathrm{x} = [\phi \quad \dot{\phi} \quad \theta \quad \dot{\theta} \quad \psi \quad \dot{\psi}]^{\mathrm{T}} \in \mathrm{R}^{\mathrm{n}}
\end{aligned} \tag{12}$$

where $n = \sum_{i=1}^{m=3} k_i = 6$ and the functions $\boldsymbol{F(x)}$ and $\boldsymbol{G(x)}$ and the vector $\boldsymbol{d}$ can be derived using Equation 9 as Equations 13 to 15

$$F(x) = [f_1(x) \quad f_2(x) \quad f_3(x)]^T \epsilon\, R^3 = \begin{bmatrix} f_1(\phi, \dot{\phi}, \theta, \dot{\theta}, \psi, \dot{\psi}) \\ f_2(\phi, \dot{\phi}, \theta, \dot{\theta}, \psi, \dot{\psi}) \\ f_3(\phi, \dot{\phi}, \theta, \dot{\theta}, \psi, \dot{\psi}) \end{bmatrix} \tag{13}$$

$$G = \begin{bmatrix} \frac{1}{I_{xx}} & \frac{\sin\theta\sin\phi}{I_{yy}\cos\theta} & \frac{\cos\phi\sin\theta}{I_{zz}\cos\theta} \\ 0 & \frac{\cos\phi}{I_{yy}} & -\frac{\sin\phi}{I_{zz}} \\ 0 & \frac{\sin\phi}{I_{yy}\cos\theta} & \frac{\cos\phi}{I_{zz}\cos\theta} \end{bmatrix} \tag{14}$$

$$\boldsymbol{d} = \begin{bmatrix} \frac{T_{dis\,x}}{I_{xx}} & \frac{T_{dis\,y}}{I_{yy}} & \frac{T_{dis\,z}}{I_{zz}} \end{bmatrix}^T \tag{15}$$

In the above equations, $\mathrm{F(x)} = [\mathrm{f_1(x)} \quad \mathrm{f_2(x)} \quad \mathrm{f_3(x)}]^{\mathrm{T}} \epsilon\, \mathrm{R}^3$ denotes the subsystem equations of the satellite, which are all smooth and frequently unknown functions of the measurable state variables. Subsequently, G is an unknown positive definite matrix for which G^{-1} must always exist and finally, $\boldsymbol{d} = [d_1 \quad d_2 \quad d_3]^T \epsilon R^3$ is the uncertainty vector of the system, where the condition

$|d_i| \leq \delta$ must hold for all positive and finite δ numbers. A brief description of the vector $\boldsymbol{d}$ components is provided in Appendix A.

2-2- Reaction Wheels Stabilization

Among various actuators, reaction wheels are preferred when high precision, relatively fast, and smooth responses are required. For simulation purposes, the output torque is assumed to be limited to 2 N.m [11].

In some cases, passive stabilization devices are combined with active ones to create a semi-active stabilization system. However, the use of a gravity gradient boom alongside reaction wheels is uncommon for two key reasons:

1. Mounting the reaction wheels on three sides of the satellite occupies positions that would typically be suitable for installing a gravity gradient boom.

2. The performance of a gravity gradient boom is significantly inferior to that of reaction wheels.

Nevertheless, in specific scenarios, one or two (low-power) reaction wheels are added to a gravity gradient boom to enhance its stabilization performance [12].

For this study, it is assumed that three reaction wheels, aligned with the satellite's principal axes, are used. Each reaction wheel consists of a coaxial electric motor and a flywheel and operates according to the principle of angular momentum conservation.

A DC motor drives each reaction wheel. When the control unit provides the required torque component as a command signal, the motor's linear controller adjusts the angular velocity of the rotor ω_m to achieve the desired angular velocity of the reaction wheel $\boldsymbol{\omega}_r$. For each reaction wheel, the relationship $\mathrm{J_m \omega_m = J_w \omega_w}$ holds. Assuming negligible lateral disturbances around the reaction wheel, this relationship is consistent with the principle of angular momentum conservation as Equation 16 [11]

$$\dot{\boldsymbol{h}}_w + \dot{\boldsymbol{h}}_s = 0 \tag{16}$$

According to Equation 16, applying mechanical torque to the satellite body in one direction results in producing an equal torque in the opposite direction by the electric motor, as shown by Equation 17

$$\dot{\boldsymbol{h}}_s = -\dot{\boldsymbol{h}}_w = -\dot{\boldsymbol{h}}_m \tag{17}$$

The dynamics of the servo motors of each reaction wheel can be expressed as Equation 18 [13]

$$\frac{d}{dt}\begin{bmatrix} \Theta \\ \omega_w \\ i \end{bmatrix} = \begin{bmatrix} 0 & 1 & 0 \\ 0 & 0 & \frac{Nk_m}{J_e} \\ 0 & -\frac{Nk_m}{L} & -\frac{\Re}{L} \end{bmatrix}\begin{bmatrix} \Theta \\ \omega_w \\ i \end{bmatrix} + \begin{bmatrix} 0 & 0 \\ 0 & -\frac{1}{J_e} \\ \frac{1}{L} & 0 \end{bmatrix}\begin{bmatrix} v \\ T_L \end{bmatrix} \tag{18}$$

where Θ represents the rotation angle of each reaction wheel, $\boldsymbol{T}_L$ is the desired amount of torque input as a control signal, k_m is a relationship coefficient between motor torque and the electric current, and $\boldsymbol{J}_e$ is the effective moment of inertia. Also, for each reaction wheel, the elements of Equation 18 could be expressed as Equations 19 and 20.

$$\boldsymbol{T}_m = K_m i \tag{19}$$

$$\boldsymbol{J}_e = \boldsymbol{J}_w + N^2 \boldsymbol{J}_m \tag{20}$$

where $\boldsymbol{J}_m$ and $\boldsymbol{J}_w$ are the moments of inertia of the motor and the reaction wheel, respectively.

3- Controller Design

3-1- Fuzzy Sliding Mode Controller

Starting with the standardized Equation 11, a sliding mode controller is initially designed. In subsequent steps, fuzzy and adaptive rules are incorporated to enhance its performance. The three sliding surfaces of the system can be shown as Equation 21 [13]

$$\begin{gathered} S_i = \lambda_i^T \tilde{Y}_i \quad , \quad i = 1,2,3 \ (m = 3) \\ \boldsymbol{\lambda}_i = \left[\lambda_{i1}, \dots, \lambda_{i(k_i-1)}, 1\right]^T \quad , \quad \tilde{\boldsymbol{Y}}_i = \left[\tilde{y}_i, \dots, \tilde{y}_i^{(k_i-1)}\right]^T \\ \tilde{\boldsymbol{y}} = \boldsymbol{y}_d - \boldsymbol{y}_i \quad , \quad \boldsymbol{y}_d = [y_{d1} \quad y_{d2} \quad y_{d3}]^T \end{gathered} \tag{21}$$

The sliding mode law is defined as Equation 22, where $\boldsymbol{u}_{eq}^*$ is derived using Equation 11 and $\dot{\boldsymbol{s}} = 0$. Finally, $\boldsymbol{u}_{rb}$ is designed to dispel the uncertainties [14].

$$\begin{gathered} \boldsymbol{\lambda}_i = [\lambda_{i1}, 1]^T \quad , \quad \tilde{\boldsymbol{Y}}_i = [\tilde{y}_i, \dot{\tilde{y}}_i]^T \\ \boldsymbol{u} = \boldsymbol{u}_{eq}^* + \boldsymbol{u}_{rb} \\ \boldsymbol{u}_{eq}: \dot{\boldsymbol{s}} = 0 \\ \dot{\boldsymbol{s}} = \boldsymbol{E}_\lambda - \boldsymbol{F}(\boldsymbol{x}) - G\boldsymbol{u} - \boldsymbol{d} + \boldsymbol{y}_d^{(2)} \\ \Rightarrow \ \boldsymbol{u}_{eq}^* = G^{-1}\left(\boldsymbol{E}_\lambda - \boldsymbol{F}(\boldsymbol{x}) - \boldsymbol{d} + \boldsymbol{y}_d^{(2)}\right) \\ \boldsymbol{u}_{rb} = G^{-1}[K sgn(\boldsymbol{s})] \end{gathered} \tag{22}$$

And the element of $\boldsymbol{E}_\lambda$ in Equation 22 could be defined as Equation 23

$$\boldsymbol{E}_\lambda = \sum_{j=1}^{(k-1)} \lambda_{ij} \tilde{y}_i^{(j)} \quad , \quad k = 2 \tag{23}$$

The sliding mode control law comprises two components: an equivalent input that guides the system towards the sliding surface and a robust input that maintains the system on the sliding surface. The sliding mode control law comprises two components: an equivalent input that guides the system towards the sliding surface and a robust input that maintains the system on the sliding surface. To reduce the chattering effect caused by the sign function, the substitution of $K_i sgn(s_i) \rightarrow K_{rb\,i} \frac{s_i}{\sqrt{|s_i|^2+\beta}}$ has been performed in Equation 22, in which the Krb coefficient and the β constant are chosen by manual trial and error.

In the SMC controller design, the calculated $\boldsymbol{u}$ from Equation 22 is used as the control input, $\boldsymbol{T}$, in Equation 9.

$\boldsymbol{u}_{eq}^*$ represents the ideal equivalent sliding-mode control input, which is unattainable due to system uncertainties and the incomplete information about the system. To approximate $\boldsymbol{u}_{eq}^*$, a fuzzy system with n_i inputs and one output is employed, based on n_r fuzzy (IF-THEN) rules. The output of each fuzzy subsystem is calculated as Equation 24 [14]

$$\begin{aligned} u_i' &= \boldsymbol{b}_i^T \boldsymbol{w}_i \\ \boldsymbol{b}_i &= \left[b_i^1, \dots, b_i^{n_r}\right]^T \\ \boldsymbol{w}_i &= \left[w_i^1, \dots, w_i^{n_r}\right]^T \end{aligned} \tag{24}$$

where $\boldsymbol{b}_i$ is the rth component of the fuzzy coefficient vector, and $\boldsymbol{w}_i$ gives the coefficient intensity vector of each rule as Equation 25

$$w_i^r = \frac{\prod_{j=1}^{n_i} \mu_{A_j^r(x_j)}}{\sum_{r=1}^{n_r} \prod_{i=1}^{n_i} \mu_{A_i^j(x_i)}} \tag{25}$$

and $\boldsymbol{A}^r = [A_1^r, \dots, A_{\mathrm{ni}}^r]$ is the fuzzy set of r's law denoted by Gaussian membership functions calculated as Equation 26

$$w_i^r = \frac{\prod_{j=1}^{n_i} \mu_{A_j^r(x_j)}}{\sum_{r=1}^{n_r} \prod_{i=1}^{n_i} \mu_{A_i^j(x_i)}} \tag{26}$$

A fuzzy set based on five rules has been employed for the intended satellite control. So, for a system with five fuzzy rules, $r = 5$ and the elements of fuzzy rules are presented as Equation 27

$$\boldsymbol{b}_m = \left[b_i^1, \dots, b_i^5\right]^T \quad , \quad \boldsymbol{w}_m = \left[w_i^1, \dots, w_i^5\right]^T \tag{27}$$

The parameters and conditions used in the fuzzy rules for the simulation are presented in Table (1).

Table (1) : The parameters of the fuzzy rules

Parameters	Values
$\boldsymbol{B}_i^{r\,T}, r = 1,2,3,4,5$	[1 1 1 1 1]
$\sigma_j^r, r = 1,2,3,4,5$	0.05
c_j^1	-0.3
c_j^2	-0.15
c_j^3	0
c_j^4	0.15
c_j^5	0.3

The estimated fuzzy input for $\boldsymbol{u}_{eq}^*$ is calculated by creating the m input - m output normalization matrix P, with members denoted by p_{ij} and could be calculated using Equations 28 and 29 as [15]

$$\begin{aligned} u_{eq\,i}^* &= u_i^{*fuz} + \Xi_i = \sum_{j=1}^{m} P_{ij}^* u_j' + \Xi_i \\ \boldsymbol{\Xi} &= [\xi_1, \xi_2, \xi_3]^T \quad , \quad |\xi_i| < \Psi_i \end{aligned} \tag{28}$$

$$P_{ij}^* \triangleq \arg_{P_{ij}} \min \left\{ \left| \sum_{j=1}^{m} P_{ij} u_j - u_{eq\,i}^* \right| \right\} \tag{29}$$

where Ψ_i is a finite constant parameter, also $\boldsymbol{u}^{*fuz}$ and $[P^*]$ are the ideal forms of $\boldsymbol{u}^{fuz}$ and $[P]$, respectively.

Suppose $\hat{\boldsymbol{u}}^{fuz}$ as a fuzzy input for approximating $\boldsymbol{u}_{eq}^*$ and $[\hat{P}]$ as an approximation for $[P^*]$; therefore, Equation 30 is a true statement that [15]

$$\hat{\boldsymbol{u}}^{fuz} = [\hat{p}]\acute{\boldsymbol{u}} \tag{30}$$

Consequently, the control law is represented in Equation 31, as

$$\boldsymbol{u} = \hat{\boldsymbol{u}}^{fuz} + \boldsymbol{u}^{rb}, \quad \boldsymbol{u}^{rb} = diag(\hat{\boldsymbol{\Psi}}) sgn(\boldsymbol{s}) \tag{31}$$

where $\hat{\boldsymbol{u}}^{fuz}$ is an approximation for $\boldsymbol{u}_{eq}^*$, and the uncertainties of this approximation are mitigated by $\boldsymbol{u}^{rb}$. The variable $\widehat{\Psi}$ and the matrix $[\hat{P}]$ should be estimated using adaptive laws derived from the Lyapunov stability criterion.

3-2- Adaptive Rules and Stability Analysis [10, 14]

The Lyapunov function $V(s,\tilde{P},\widetilde{\Psi})$ is assumed as Equation 32, where $[\tilde{P}]$ and $\widetilde{\Psi}$ are calculated as Equation 33

$$V(s,\tilde{P},\widetilde{\Psi}) = \frac{1}{2}s^T G^{-1} s + \frac{1}{2\gamma}\sum_{i=1}^{m}\sum_{j=1}^{m}\tilde{P}_{ij}\tilde{P}_{ij} + \frac{1}{2\alpha}\sum_{i=1}^{m}\widetilde{\Psi}_i\widetilde{\Psi}_i \quad (32)$$

$$\widetilde{\Psi}_i = \Psi_i - \widehat{\Psi}_i$$
$$\tilde{P}_{ij} = P_{ij}^* - \hat{P}_{ij} \quad (33)$$

and $\dot{\boldsymbol{s}}$ can be written out as shown in Equation 34, using Equation 22 and Equation 31

$$\dot{\boldsymbol{s}} = \boldsymbol{E}_\lambda - \boldsymbol{F}(\boldsymbol{x}) - G(\hat{\boldsymbol{u}}^{fuz} + \boldsymbol{u}^{rb}) - \boldsymbol{d} + \boldsymbol{y}_d^{(2)}$$
$$\rightarrow G^{-1}\dot{\boldsymbol{s}} = G^{-1}(\boldsymbol{E}_\lambda - \boldsymbol{F}(\boldsymbol{x}) - \boldsymbol{d} + \boldsymbol{y}_d^{(2)}) - (\hat{\boldsymbol{u}}^{fuz} + \boldsymbol{u}^{rb})$$
$$\rightarrow \dot{\boldsymbol{s}} = G(\boldsymbol{u}^* - \hat{\boldsymbol{u}}^{fuz} - \boldsymbol{u}^{rb}) \quad (34)$$

The Lyapunov criterion according to Equation 32 and Equation 34 is expressed as Equation 35

$$\dot{V}(s,\tilde{P},\widetilde{\Psi}) = \sum_{i=1}^{m} s_i(\tilde{u}_i^{fuz} + \xi_i - u_i^{rb}) + \frac{1}{\gamma}\sum_{i=1}^{m}\sum_{j=1}^{m}\tilde{P}_{ij}\dot{\tilde{P}}_{ij} + \frac{1}{\alpha}\sum_{i=1}^{m}\widetilde{\Psi}_i\dot{\widetilde{\Psi}}_i$$
$$= \sum_{i=1}^{m}\sum_{j=1}^{m} s_i(\tilde{P}_{ij}u_j' + \xi_i - u_i^{rb}) + \frac{1}{\gamma}\overbrace{\sum_{i=1}^{m}\sum_{j=1}^{m}\tilde{P}_{ij}\dot{\tilde{P}}_{ij}}^{\dot{\tilde{P}}_{ij}=-\gamma s_i u_j'} + \frac{1}{\alpha}\overbrace{\sum_{i=1}^{m}\widetilde{\Psi}_i\dot{\widetilde{\Psi}}_i}^{\dot{\widetilde{\Psi}}_i=-\alpha s_i}$$
$$= \sum_{i=1}^{m}[s_i(\xi_i - \widehat{\Psi}_i sgn(s_i)) - \widetilde{\Psi}_i|s_i|]$$
$$= \sum_{i=1}^{m}[s_i\xi_i - |s_i|(\widehat{\Psi}_i + \widetilde{\Psi}_i)]$$
$$= \sum_{i=1}^{m}(s_i\xi_i - |s_i|\widehat{\Psi}_i) \le \sum_{i=1}^{m}(|s_i||\xi_i| - |s_i|\widehat{\Psi}_i)$$
$$= -\sum_{i=1}^{m}|s_i|(\widehat{\Psi}_i - |\xi_i|) \le 0 \Rightarrow \dot{V}(s,\tilde{P},\widetilde{\Psi}) \le 0 \quad (35)$$

According to Equation 35 and using the approximation errors provided in Equation 33, the stability of the system can be guaranteed by setting the parameter Ψ and the matrix $[P]$ as Equation 36

$$\dot{\hat{P}}_{ij} = -\dot{\tilde{P}}_{ij} = \gamma s_i(t)\acute{u}(j)$$
$$\dot{\widehat{\Psi}}_i = -\dot{\widetilde{\Psi}}_i = \alpha|s_i(t)| \quad , \quad i,j = 1,2,3 \quad (36)$$

To achieve the desired frequency range and convergence rate, the two positive coefficients, α and γ in Equation 36, are tuned through trial and error.

When the adaptive conditions are met, Equation 35 yields a negative semi-definite function $\dot{V}(\boldsymbol{s},\tilde{P},\widetilde{\Psi})$, thereby confirming the stability of the system.

Assuming that Equation 37 is correct and integrating its two sides, the Equation 38 is obtained as follows

$$\Gamma = \sum_{i=1}^{m=3}|s_i|(\widehat{\Psi}_i - |\xi_i|) \le -\dot{V} \quad (37)$$

$$\int_0^t \Gamma(\tau)d\tau = V(s_i(0),\tilde{P},\widetilde{\Psi}) - V(s_i(t),\tilde{P},\widetilde{\Psi}) \quad (38)$$

Given that $V(s_i(0),\tilde{P},\widetilde{\Psi})$ has a finite value and $V(s_i(t),\tilde{P},\widetilde{\Psi})$ does not increase over time, the Equation 39 can be deduced that

$$\lim_{t\to\infty}\int_0^t \Gamma(\tau)d\tau < \infty \quad (39)$$

Considering Equation 39 and according to the Barbalat lemma, $\dot{\Gamma}(\tau)$ has a finite value, and if $\lim_{t\to\infty} s_i = 0$ holds in Equation 37, then $\lim_{t\to\infty}\Gamma_i = 0$ also holds; therefore, the proposed system is asymptotically stable.

4- Communication Device

The selection of an appropriate antenna for a communication satellite is influenced by its altitude, orbit, and the required task precision. The antenna must emit a wave with suitable characteristics.

A mission implementation coefficient quantifies the acceptable pointing error for a satellite. In communication satellites, this error is expressed as a coefficient of the Half Power Beam Width angle, denoted by θ_{HPBW}, where the relative antenna power is marginally greater than 50% of the peak power in the effective radiated field. This angle can be approximately given by Equation 40 as [16]

$$\Theta_{HPBW} = 65^\circ\frac{\lambda}{D} \quad (40)$$

As indicated by Equation 40, larger satellite antenna apertures result in narrower beam widths and HPBW angles, thereby improving pointing precision [16].

In this study, Ka-band transmission is assumed to enable faster information dissemination via direct signals. Furthermore, a sun sensor with 0.02 degrees accuracy and a 4cm aperture antenna with a 1cm transmitter wavelength are employed. Based on Equation 40, the desired wave will reach the ground receiver with a 3dB power loss at a 16.25-degree propagation angle, and the allowable pointing error will be a small fraction of this angle.

According to Chahat et al. [17], a communication satellite transmitting signals to Earth with the same HPBW angle (3dB power loss) can tolerate a pointing error of 0.5 degrees. This critical design parameter for controllers is used to evaluate controller efficiency in simulations. The selected sensor can also measure the achieved pointing precision.

5- Results and Discussion

Before implementing the controller, the satellite's uncontrolled dynamic behavior is analyzed under ideal initial conditions. The allowable attitude deviation is set to 0.5 degrees, triggering controller and actuator activation once this threshold is reached. Figure (1-A) shows that, in the absence of disturbances, the yaw angle gradually diverges from its ideal state. Conversely, Figure (1-B) illustrates that, under the influence of disturbances, the roll and pitch angles exhibit quasi-oscillatory deviations. In contrast, the yaw angle exceeds the 0.5-degree threshold after approximately 502 seconds, prompting the engagement of the controller and actuator.

The Keplerian orbital elements of the satellite considered in this paper are presented in Table (2).

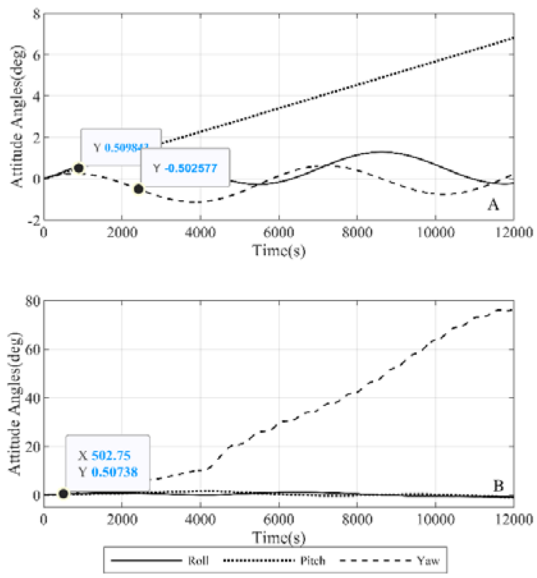

Figure (1) : Satellite attitude changing over time with no controlling conditions; A: Regardless of the disturbing torques, B: With disturbing torques

5-1- Comparison of Small Angle Simulation Results

Satellite dynamics are inherently nonlinear, often requiring advanced control algorithms for effective management. While linearization techniques are commonly used to approximate nonlinear systems for linear controllers, these approximations can introduce significant errors, particularly in complex systems. As a result, linear control methods such as PD and PID are generally effective only for small initial deviations.

To demonstrate the performance differences between linear and nonlinear approaches, this study compares the AFSMC method with PD and SMC controllers under both small and large deviation conditions. The key parameters for controlling the satellite in small deviation scenarios are provided in Table (3).

Table (2) : The Keplerian elements of the satellite

Parameters	Values
E	0
H (km)	1000
T (sec)	6307.3
$\Omega\ (deg)$	40
i (deg)	83
$\omega\ (deg)$	30

Figure (2), Figure (3), and Figure (4) illustrate the attitude control of initial deviations in roll, pitch, and yaw angles under small angle conditions. The PD method exhibits overshoot in both roll and pitch angles, whereas the SMC and AFSMC methods show no overshoot

Table (3) : Small deviation control parameters for regenerating PD, SMC and AFSMC algorithms

Parameters	Values	Parameters	Values
δt (sec) = 0.025	0.025	$(\dot{\phi}_0, \dot{\theta}_0, \dot{\psi}_0)$ (rad/sec)	(1, 1, 1)$\times 10^{-5}$
$\boldsymbol{I_{sat}}$ (kg.m^2)	Diag (2.451 2.451 2.194)	(α, γ)	(6,0.00001)
m_{sat} (kg)	67	β	0.02
$(\dot{\phi}_{0\,des}, \dot{\theta}_{0\,des}, \dot{\psi}_{0\,des})$ (rad/sec)	(0, 0, 0)	$(K_{rb1}, K_{rb2}, K_{rb3})$	(0.032, 0.015, 0.015)
$(\phi_{0\,des}, \theta_{0\,des}, \psi_{0\,des})$ (rad)	(0, 0, 0)	$(\lambda_1, \lambda_2, \lambda_3)$ for SMC	(0.7, 0.9, 0.7)
$\boldsymbol{I_{RW}}$ (kgm^2)	Diag (2.2018 2.2018 2.2018)$\times 10^{-4}$	$(\lambda_1, \lambda_2, \lambda_3)$ for AFSMC	(0.7,0.9,0.7)
$\boldsymbol{h_W}_{(max)}$ (N.m.s)	(0.025, 0.025, 0.025)	(P_{Roll}, D_{Roll})	(0.03000,0.41461)
Ψ_{io} , $i = 1،2،3$	0	(P_{Pitch}, D_{Pitch})	(0.01326,0.06565)
p_{ij0} , $i,j = 1،2،3$	0	(P_{Yaw}, D_{Yaw})	(0.48724,0)
$(\phi_0, \theta_0, \psi_0)$ (rad)	(-0.0087, 0.01, 0.0087)		

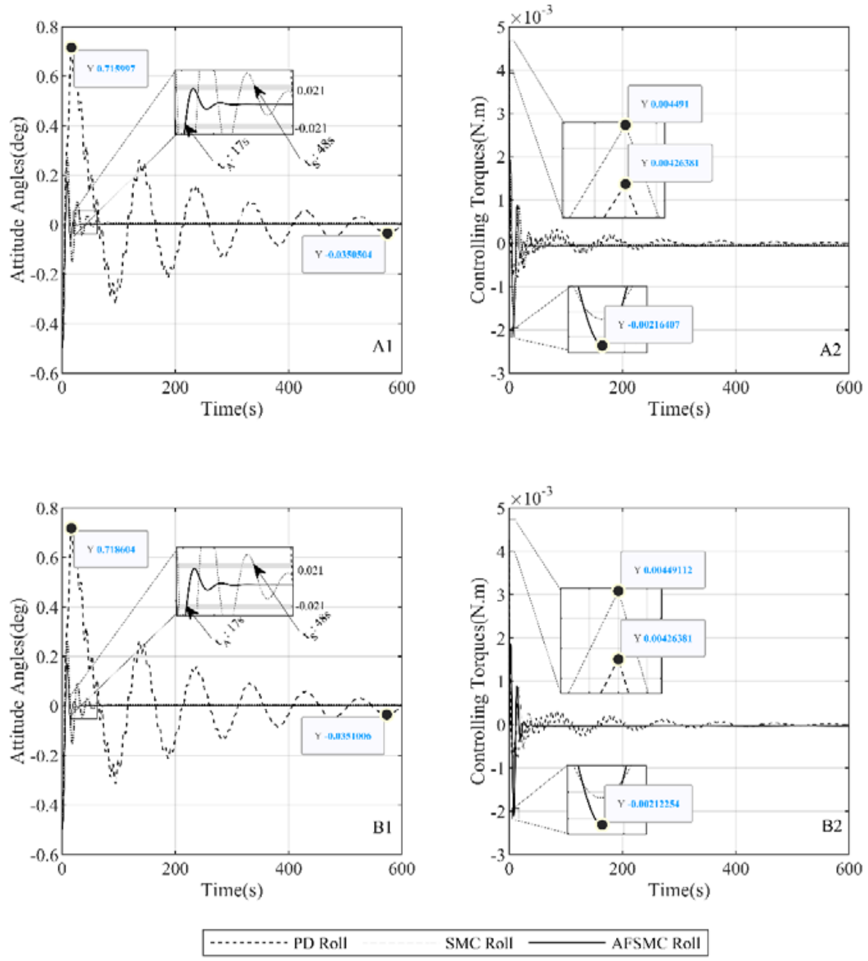

Figure (2) : The comparison of Roll angle deviations control for the small initial deviations condition between three control methods; A1: controlled Roll angle – No disturbance, A2: Roll angle control torques – No disturbance, B1: controlled Roll angle – Disturbance added, B2: Roll angle control torques – Disturbance added.

Given a measurement accuracy of 0.02 degrees, as discussed in section 4, the SMC and AFSMC methods achieve settling times of under 60 seconds for all three attitude angles. In contrast, the PD method fails to reach the settling range within 600 seconds at any angle.

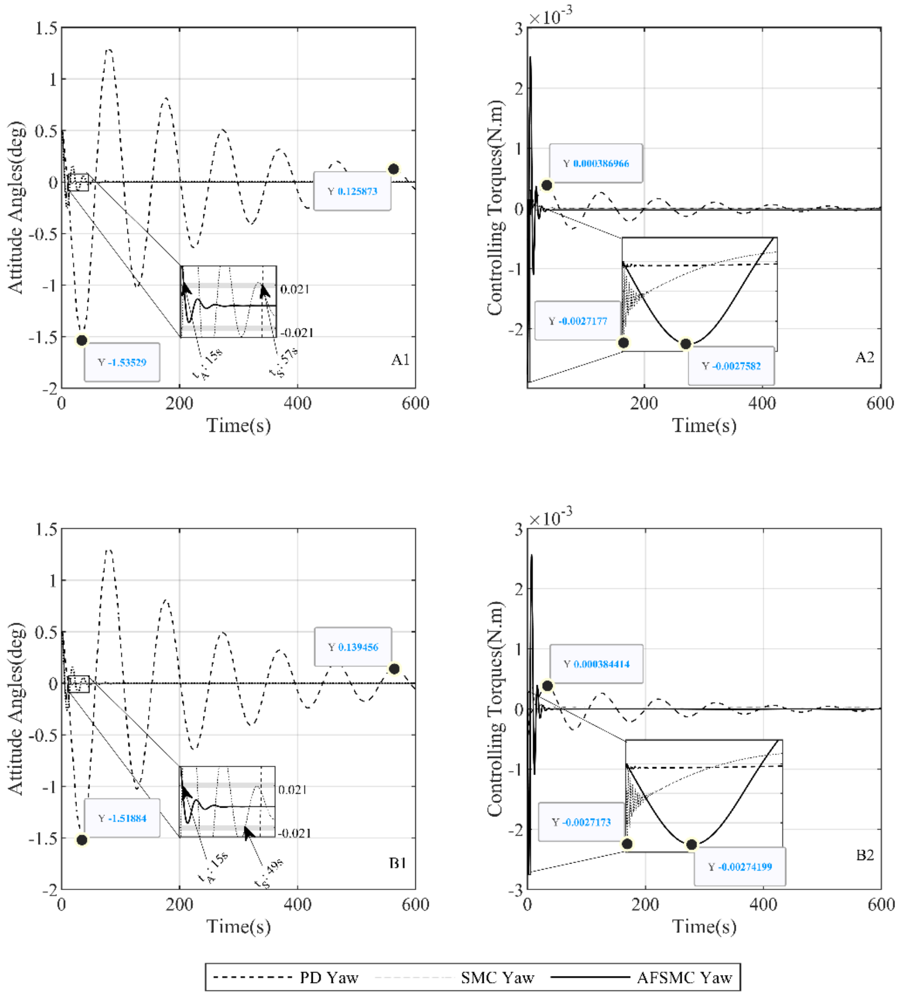

Figure (3) : The comparison of Pitch angle deviations control for the small initial deviations condition between three control methods; A1: controlled Pitch angle – No disturbance, A2: Pitch angle control torques – No disturbance, B1: controlled Pitch angle – Disturbance added, B2: Pitch angle control torques – Disturbance added.

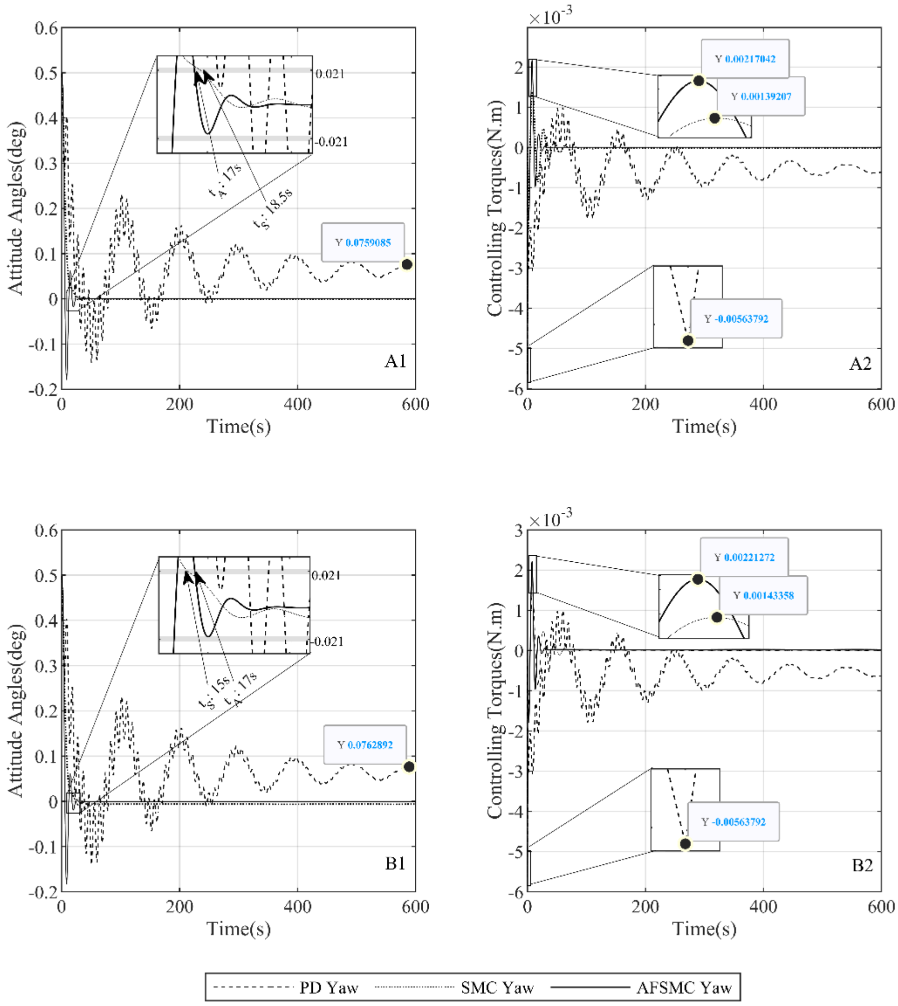

Figure (4) : The comparison of Yaw angle deviations control for the small initial deviations condition between three control methods; A1: controlled Yaw angle – No disturbance, A2: Yaw angle control torques – No disturbance, B1: controlled Yaw angle – Disturbance added, B2: Yaw angle control torques – Disturbance added.

Notably, the AFSMC method outperforms the SMC method, achieving stabilization within 20 seconds at all three attitude angles. Furthermore, Figures (2-4) indicate that the AFSMC method achieves the desired attitude angles with lower control torque compared to the other two methods.

What was observed in Figures (2-4) regarding the performance of the three control algorithms is summarized in Table (4).

The effects of disturbances are minimal across all controllers. Figure (5) shows that disturbance torques, for both small and large deviations, fluctuate with negligible amplitudes on the order of 1e-6, making them insignificant compared to control torques, particularly at larger angles. Consequently, disturbances were omitted from the large angle deviation simulations.

Table (4) : A brief comparison of the performance of three control scenarios in two conditions of applying disturbances and ignoring them, in the case of small deviations

		Roll				Pitch				Yaw			
		t_s (s)	e_{ss} (deg)	T_{max} (N.m)	M_P (deg)	t_s (s)	e_{ss} (deg)	T_{max} (N.m)	M_P (deg)	t_s (s)	e_{ss} (deg)	T_{max} (N.m)	M_P (deg)
Without Disturbances	PD	---	-350 e(-4)	43 e(-7)	0.716	---	0.1259	39 e(-8)	-1.53	---	0.0759	-56 e(-7)	0.4017
	SMC	48	73 e(-4)	45 e(-7)	0.271	57	37 e(-4)	-27 e(-7)	-0.254	18.5	-7 e(-4)	14 e(-7)	34 e(-4)
	AFSMC	17	27 e(-4)	-22 e(-7)	0.177	15	10 e(-4)	-28 e(-7)	-0.153	17	-1 e(-4)	22 e(-7)	-0.179
With Disturbances	PD	---	-351 e(-4)	43 e(-7)	0.718	---	0.1395	38 e(-8)	-1.52	---	0.0763	-56 e(-7)	0.4034
	SMC	48	40 e(-4)	45 e(-7)	0.265	49	(-4,5) e(-4)	-27 e(-7)	-0.261	15	-(56,66) e(-4)	14 e(-7)	-77 e(-4)
	AFSMC	17	16 e(-4)	-21 e(-7)	0.174	15	-7 e(-5)	-27 e(-7)	-0.157	17	-15 e(-4)	22 e(-7)	-0.183

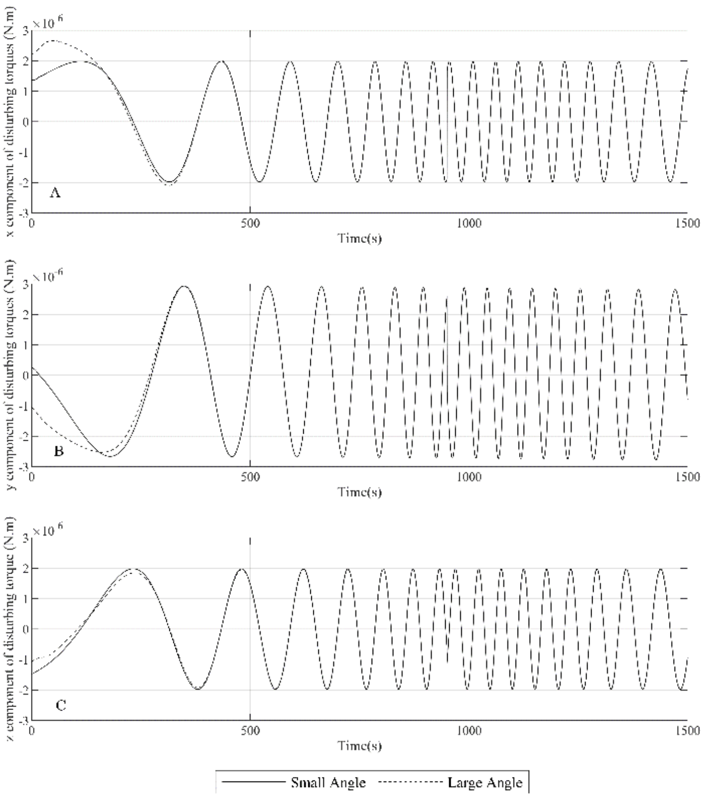

Figure (5) : Disturbing torques changing with time for the conditions of small and large initial deviations

5-2- Comparison of Large Angle Simulation Results:

After demonstrating satisfactory performance under small deviation conditions, the AFSMC controller is evaluated for large initial angle deviations. The control parameters for this scenario are provided in Table (5).

For large-angle initial deviations, the desired final attitude, as outlined in Section 4, is set at 0.5 degrees. As shown in Figure (6), the AFSMC method achieves a shorter settling time compared to the SMC method for all attitude angles except pitch. Conversely, the PD controller fails to reach the settling state or the desired value for any attitude angle except roll.

Furthermore, the PD method exceeds the allowable control torque limits of the selected reaction wheels. The performance of the three control algorithms has been shown in Figure (6) and is summarized in Table (6).

Table (5) : Large deviation control parameters for regenerating PD, SMC and AFSMC algorithms

Parameters	Values	Parameters	Values
$(\dot{\phi}_{0\,des}, \dot{\theta}_{0\,des}, \dot{\psi}_{0\,des})$ (rad/sec)	(0, 0, 0)	β	0.02
$(\phi_{0\,des}, \theta_{0\,des}, \psi_{0\,des})$ (rad)	(0, 0, 0)	$(K_{rb1}, K_{rb2}, K_{rb3})$	(0.01, 0.01, 0.01)
ψ_{io} , $i = 1،2،3$	0	$(\lambda_1,\lambda_2, \lambda_3)$ for SMC	(0.01, 0.01, 0.016)
p_{ijo} , $i,j = 1،2،3$	0	$(\lambda_1,\lambda_2، \lambda_3)$ for AFSMC	(0.01,0.01,0.016)
$(\phi_0, \theta_0, \psi_0)$ (rad)	(-0.0087, 0.01, 0.0087)	(P_{Roll}, D_{Roll})	(0.03000,0.41461)
$(\dot{\phi}_0, \dot{\theta}_0, \dot{\psi}_0)$ (rad/sec)	(1, 1, 1)$\times 10^{-5}$	(P_{Pitch}, D_{Pitch})	(0.01326,0.06565)
(α, γ)	(0.7,0.00001)	(P_{Yaw}, D_{Yaw})	(0.48724,0)

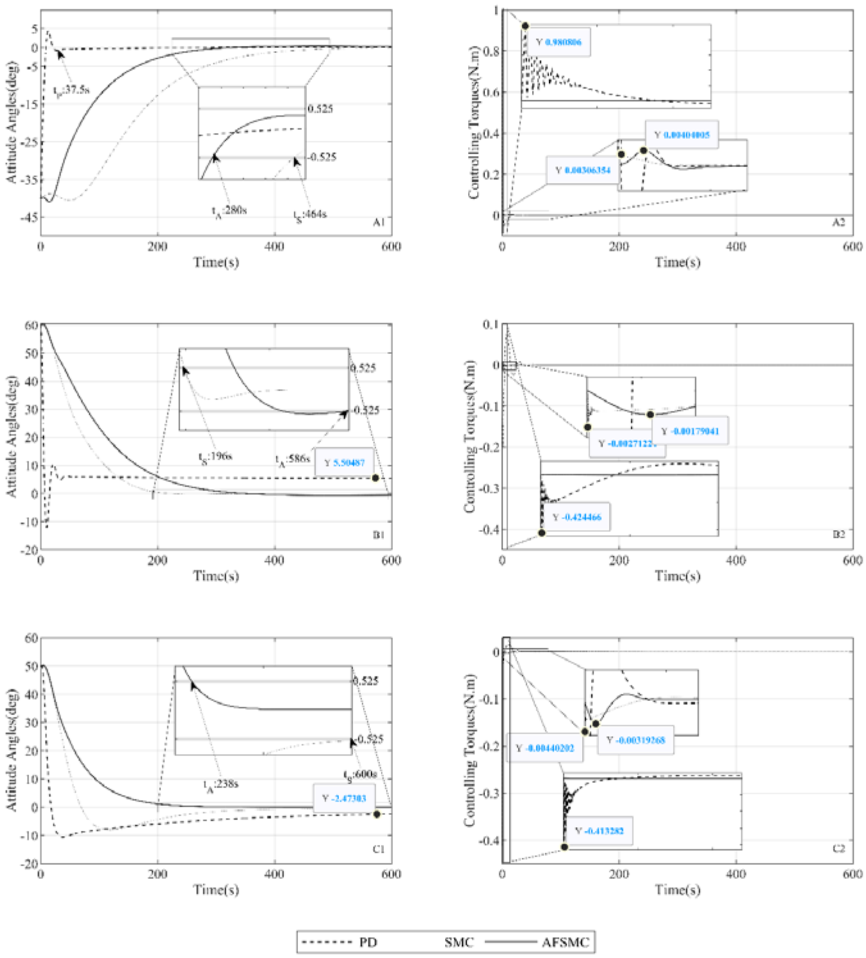

Figure (6) : The comparison of three control methods in the large angle deviations condition; A1: controlled Roll angle, A2: Roll angle control torques, B1: controlled Pitch angle, B2: Pitch angle control torques, C1: controlled Yaw angle, C2: Yaw angle control torques.

Table (6) : A brief comparison of the performance of three control scenarios in the case of large deviations

	Roll				Pitch				Yaw			
	t_s (s)	e_{ss} (deg)	T_{max} (N.m)	M_P (deg)	t_s (s)	e_{ss} (deg)	T_{max} (N.m)	M_P (deg)	t_s (s)	e_{ss} (deg)	T_{max} (N.m)	M_P (deg)
PD	37.5	0.110	0.9808	4.475	---	5.499	-0.4245	-12.153	---	-2.473	-0.4133	-10.610
SMC	464	-0.080	0.0031	-40.539	196	8 e(-5)	-0.0027	---	238	-0.515	-0.0044	-7.932
AFSMC	280	0.350	0.0040	-40.948	586	-0.162	-0.0018	---	600	0.005	-0.0032	---

As illustrated in Error! Reference source not found.**)**, the AFSMC method achieves the desired attitude angles while consuming less control energy compared to both PD and SMC controllers.

As expected, the linear PD control method proved inadequate for managing large deviations, failing to achieve the required precision. While the SMC method demonstrated relatively acceptable performance for large-angle attitude control, the AFSMC method outperformed it in terms of accuracy, speed, and energy efficiency.

6- Conclusion

This paper explores the application of Adaptive Fuzzy Sliding Mode Control (AFSMC) for the attitude control of a low Earth orbit (LEO) communication satellite equipped with three reaction wheels. Due to the system's complexity and inherent uncertainties, AFSMC is chosen for its robustness against unknown disturbances, simplicity, speed, accuracy, and ability to ensure convergence to a steady state.

To demonstrate the advantages of the AFSMC approach, its performance is compared with that of the Proportional-Derivative (PD) and Sliding Mode Control (SMC) methods under identical conditions. Simulation results indicate that the PD controller fails to meet the design requirements, whereas the SMC method delivers reasonable performance. However, the AFSMC method outperforms both, offering superior accuracy, faster response times, and greater energy efficiency, all without relying on precise system dynamics. To achieve the desired frequency range and convergence rate, the two positive coefficients, α and γ, in Equation 36 can be trained more systematically; a method for their optimal tuning is provided in Mousavi et al. [18]. The method is based on reinforcement learning and will be employed in future studies.

In conclusion, the proposed AFSMC controller effectively meets the research objectives, enabling the satellite to achieve the desired state under optimal conditions, thereby validating its suitability for robust attitude control.

Funding and Competing Interests

No funds, grants, or other support were received, and the authors have no financial or proprietary interests in any material discussed in this article.

Nomenclature			
Parameter	**Description**	**Parameter**	**Description**
$[\phi \quad \theta \quad \psi]^T$(rad)	Euler angles	$R_o\ (m)$	Radius of orbit
$\omega_o(\frac{rad}{s})$	Satellite orbit angular velocity	$c\ (\frac{m}{s})$	Speed of light
$M\ (kg)$	Total mass of the Earth	$\boldsymbol{h}\ (N.m.s)$	Angular momentum vector
C_D	Satellite coefficient of drag	R_1, R_2, R_3	Nonlinear functions for satellite attitude dynamics
$\Lambda\ (rad)$	Satellite latitude	$\boldsymbol{D}_{S/C}(A.m^2)$	The spacecraft's effective magnetic moment
$\boldsymbol{B}_O\ \left(\frac{wb}{m^2}\right)$	The geocentric magnetic flux density	$D(m)$	Antenna's aperture diameter
$\lambda\ (m)$	Wavelength of transmitted signal	$i\ (A)$	Servo motor current
N	Gear conversion ratio	$\Re\ (\Omega)$	Servo motor resistance
$L\ (H)$	Servo motor inductance	v (v)	Voltage applied to servo motor
$\boldsymbol{J}\ (kg.m^2)$	Moment of inertia	$\alpha\ ,\gamma$	AFSMC learning rates
(c, σ)	Center and width of fuzzy membership functions	$\mu_{A_i^r}$	Fuzzy membership functions
μ (=GM) ($m3{\cdot}s^{-2}$)	The geocentric gravitational constant	$\boldsymbol{\omega}(\frac{rad}{s})$	Angular velocity vector

$\boldsymbol{I}\ (kg.m^2)$	Moment of inertia matrix	$\boldsymbol{T}\ (Nm)$	Torque vector
$dA\ (m^2)$	The surface element of the satellite	$\boldsymbol{p}$	The solar radiation pressure
$\boldsymbol{V}\ (\frac{m}{s})$	The satellite orbital velocity vector relative to the atmosphere	$\rho\ (\frac{kg}{m^3})$	The atmosphere density

Subscripts			
Parameter	**Describe**	**Parameter**	**Describe**
I	Related to the ICS[1]	O	Related to the OCS[2]
B	Related to the BCS[3]	w	Related to the reaction wheel
IR	OCS relative to ICS	IB	BCS relative to ICS
RB	BCS relative to OCS	c	Related to the controller
dis	Related to disturbances	m	Related to the motor
sp	Solar pressure	eq	Equivalent
rb	Robust	T	Total
d	Desired	mag	Magnetic
$aero$	Aerodynamic	e	The effective
Superscripts			
Parameter	**Describe**	**Parameter**	**Describe**
B	Expressed in BCS	$*$	The Ideal form
fuz	Related to the fuzzy part of the controller	rb	Related to the robust part of the controller

References

[1] K. Nobuaki, N. Keiken, and S. Shigebumi, "Accuracy Improvement of Three-Axis Stabilization Using an Onboard Computer," Acta Astronautica, vol. 4, no. 9-10, pp. 1041-1058, 1977, https://doi.org/10.1016/0094-5765(77)90005-4

[2] T. Zwartbol, R. F. Van den Dam, A. P. Terpstra, and P. Th. L. M. Van Woerkom, "Attitude Estimation and Control of Manoeuvring Spacecraft," Automatica, vol. 21, no. 5, pp. 513-526, 1985, https://doi.org/10.1016/0005-1098(85)90001-9.

[3] F. F. Mobley, W. E. Radford, and L. R. Kennedy, "MSX Attitude Determination and Control Hardware," Johns Hopkins APL Technical Digest, vol. 17, no. 2, pp. 153-160, 1996.

[4] L.-H. Geng, D.-Y. Xiao, Q. Wang, T. Zhang, and J.-Y. Song, "Attitude-control model identification of on-orbit satellites actuated by reaction wheels," Acta Astronautica, vol. 66, no. 5-6, pp. 714-721, 2010, https://doi.org/10.1016/j.actaastro.2009.08.013.

[5] M. R. Alipour, F. Fani Saberi, and M. Kabganian, "Modelling, Design, and Experimental Implementation of Non-linear Attitude Tracking with Disturbance Compensation Using Adaptive Sliding Control Based on Quaternion Algebra," The Aeronautical Journal, vol. 122, no. 1247, pp. 1-24, 2017, https://doi.org/10.1017/aer.2017.122.

[6] Erjiang Liu, Yueneng Yang, Ye Yan, "Spacecraft attitude tracking for space debris removal using adaptive fuzzy sliding mode control", Aerospace Science and Technology, vol. 107, 2020, https://doi.org/10.1016/j.ast.2020.106310.

[7] A. E. S. Ibrahimi, A. M. Taboli, and M. A. Sultan, "Satellite Attitude Maneuver using Sliding Mode Control under Body Angular Velocity Constraints," International Journal of Computer Applications, vol. 50, no. 13, pp. 41-46, 2012.

[8] F. Fani Saberi, A. Fazlyab, and A. Ajorkar, "Design and Implementation of a Sliding Mode Attitude Controller of a Satellite in Software in the Loop Test Bed," International Journal of Computer Applications, vol. 98, no. 16, pp. 28-34, 2014, https://doi.org/10.5120/17270-7653.

[9] Duong, MD., Pham, QT., Vu, TC. et al, "Adaptive fuzzy sliding mode control of an actuator powered by two opposing pneumatic artificial muscles," Journal of Scientific Reports, vol. 13, no. 8242, 2023, https://doi.org/10.1038/s41598-023-34491-3

[10] Hao Feng, Jinye Jiang, Xiaodan Chang, at al, "Adaptive sliding mode controller based on fuzzy rules for a typical excavator electro-hydraulic position control system", Journal of Engineering Applications of Artificial Intelligence, vol. 126, Part C, 2023, https://doi.org/10.1016/j.engappai.2023.107008

[11] M. J. Sidi, Spacecraft Dynamics and Control: A Practical Engineering Approach. Cambridge, UK: Cambridge University Press, 1997.

[12] Jungju Bae, Jaeyoung Kang, "Design concepts and control algorithm to minimize the control effort for earth-orbit-raising solar sails," Journal of Aerospace Science and Technology, vol. 146, 2024, https://doi.org/10.1016/j.ast.2024.108994.

[13] P. R. Belanger, Control Engineering - A Modern Approach. Orlando, FL, USA: Saunders College Publishing, 1995.

[14] Bessa, Wallace Moreira, "An adaptive fuzzy sliding mode controller for nonlinear systems with non-symmetric dead-zone and its application to an electro-hydraulic system," 2022, arXiv preprint arXiv:2205.13669.

[15] T. Iida and H. Wakana, "Satellite Antenna," Science Direct, 2019. [Online]. Available: https://www.sciencedirect.com/topics/engineering/satellite-antenna. [Accessed: Jul. 29, 2026].

[1] Inertial Coordinate System (ECI)
[2] Orbital Coordinate System
[3] Body Coordinate System

[16] F. Aguado-Agelet, A. E. Villa, M. Arias-Acuña, and F. J. Díaz-Otero, “AOCS Requirements and Practical Limitations for High-Speed Communications on Small Satellites,” International Journal of Aerospace Engineering, vol. 2019, pp. 1-16, Feb. 2019, https://doi.org/10.1155/2019/5079738.

[17] N. Chahat, R. Hodges, J. Sauder, M. Thomson, E. Peral, and Y. Rahmat-Samii, “CubeSat Deployable Ka-band Mesh Reflector Antenna Development for Earth Science Missions,” IEEE Transactions on Antennas and Propagation, vol. 64, no. 6, pp. 2083-2093, 2016, https://doi.org/10.1109/TAP.2016.2546306.

[18] A. Mousavi, A. H. Davaie-Markazi, and A. Ferrara, “A Reinforcement Learning-Based Approach for Near-Optimal Sliding-Mode Control of Output-Constrained Uncertain Nonlinear Systems,” International Journal of Robust and Nonlinear Control, vol. 33, no. 12, pp. 6655-6674, 2023, https://doi.org/10.1002/rnc.6716.

[19] J. R. Wertz, Spacecraft Attitude Determination and Control. Dordrecht, The Netherlands: Kluwer Academic Publishers, 1978.

Appendix

A. At an orbital altitude of 1000 km, the primary disturbances affecting a satellite’s attitude are solar radiation pressure, aerodynamic drag, and the interaction between the satellite’s magnetic dipole and the Earth’s magnetic field. In this section, mathematical models for each of these disturbing factors are summarized.

a. Solar Radiation Pressure:

The solar radiation pressure torque on the satellite can be obtained as Equation A.1 [19]

$$\boldsymbol{T}_{SP} = \int \boldsymbol{R}_{SP\,i} \times d\boldsymbol{f}_{total\,i} \tag{A.1}$$

where $\boldsymbol{R}_{SP\,i}$ is the vector between the spacecraft’s center of mass and the center of pressure of the ith surface element, and the force element could be calculated as Equation A.2

$$d\boldsymbol{f}_{total} = -P\left[(1-C_s)\hat{s} + 2\left(C_s \cos\beta + \frac{1}{3}C_d\right)\hat{n}\right]\cos\beta\, dA \tag{A.2}$$

where $C_a + C_s + C_d = 1$, and $\hat{s}$ is the unit vector of the surface element towards the sun, $\hat{n}$ is the unit vector of the surface normal, and β is the angle between the unit vectors.

The torque calculated from Equation A.1 with respect to the OCS can be expressed in terms of the BCS by multiplying by $[A]$, as given in Equation 4.

b. Drag Aerodynamic Disturbing Torque

For a surface element dA, with outward normal $\hat{\boldsymbol{n}}$, the drag aerodynamic disturbing torque is given by Wertz [19] as Equation A.3

$$d\boldsymbol{f}_{aero} = -\frac{1}{2}C_D \rho \boldsymbol{V}^2 \left(\hat{n}\hat{V}_a\right)\hat{V}_a dA \tag{A.3}$$

Then the aerodynamic torque is determined as Equation A.4

$$\boldsymbol{T}_{aero} = \int \boldsymbol{r}_{aero} \times d\boldsymbol{f}_{aero} \tag{A.4}$$

where $\hat{V}_a$ is the velocity unit vector relative to the atmosphere in the same direction as $\hat{n}$ and $\boldsymbol{r}_{aero}$ is a vector from the satellite center of mass to the surface element of dA. It is sufficient to derive $\hat{V}_a$ relative to the BCS to obtain Equation 13 relative to the BCS.

Since the satellite considered in this research works at an altitude of 1000 km, the aerodynamic torque has a slight effect, and for selecting an appropriate atmospheric density value, Figure (7**)** is adequate.

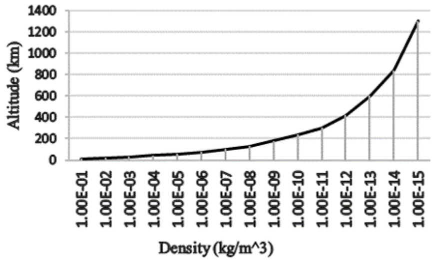

Figure (7) : Density distribution (kg⁄m^3) of the total atmosphere in terms of altitude (km) [19]

c. Magnetic Residual Disturbing Torque

The disturbing torque due to the magnetic residual dipoles in the satellite structure coils with the Earth’s magnetic field is calculated as Equation A.5 [19]

$$\boldsymbol{T}_{mag} = \boldsymbol{D}_{S/C} \times \boldsymbol{B}_o \tag{A.5}$$

where $\boldsymbol{B}_o$ is the geocentric magnetic flux density (in wb/m^2) and can be estimated in the OCS as Equation A.6

$$\boldsymbol{B}_o = B_M(\cos\Lambda, 0{,}2\sin\Lambda), B_M = \frac{7.96\times10^6}{R^3} \tag{A.6}$$

where R is the satellite geocentric distance (in km).

The torque derived from Equation A.6 can be expressed in terms of the BCS by multiplying B_o by $[A]$, as given in Equation 4.